

We are IntechOpen, the world's leading publisher of Open Access books Built by scientists, for scientists

6,900

Open access books available

186,000

International authors and editors

200M

Downloads

Our authors are among the

154

Countries delivered to

TOP 1%

most cited scientists

12.2%

Contributors from top 500 universities



WEB OF SCIENCE™

Selection of our books indexed in the Book Citation Index
in Web of Science™ Core Collection (BKCI)

Interested in publishing with us?
Contact book.department@intechopen.com

Numbers displayed above are based on latest data collected.
For more information visit www.intechopen.com



Chapter

A Practical Fitting Method Involving a Trade-Off Decision in the Parametrization Procedure of a Thermodynamic Model and Its Repercussion on Distillation Processes

Adriel Sosa, Luís Fernández, Elena Gómez, Eugénia A. Macedo and Juan Ortega

Abstract

The design of processes containing information on phase equilibria must be carried out through a series of steps, experimentation ↔ verification ↔ modeling ↔ simulation. Each of these steps should be rigorously performed to guarantee a good representation of the behavior of the system under study, whose adequate modeling could be used to simulate the corresponding process. To carry out the different previous tasks, two representative systems, extracted from known database, are used. The quality checking of experimental data series is certified through several thermodynamic consistency methods. The modeling is done by applying a multi-objective optimization procedure, which allows to define a *solution front* (*Pareto front*) for different sub-models that are established in this work. The fitness of trade-off solutions, obtained from the *efficient front*, on the design of distillation processes is analyzed through a simulation.

Keywords: multiproperty modeling, optimization procedure, trade-off decision, distillation, simulation

1. Introduction

Nowadays, process simulation [1] plays an important role in the chemical engineering field as an indispensable tool to gain precise knowledge about the process units. The use of powerful mathematical-computational tools allows to accomplish an optimal final design of chemical processes. An important matter is to ensure that the mathematical model correctly represents the quantities that reflect the state of the studied system. Then, what is a model? A model is a mathematical relationship that links the state variables of a system, such as temperature, pressure, or

compositions, influencing the process performance. Therefore, the accuracy of the selected model is essential and greatly affects the final results of the simulation and design processes. Two milestones should be considered.

The first one is the selection of the model, built-in with the mathematical relationships that best represent the variables of the system. There is no a priori a procedure to make this choice, so heuristic or experience-based criteria are generally used [2]. The second question refers to get the best parameters that complete the definition of the model for a given data series. For this latter case, there are several numerical procedures [3, 4] that allow to address the problem to optimize the parameter set considering the starting hypothesis.

The thermodynamic properties having the greatest influence on the simulation of separation processes are those related to phase equilibria (vapor-liquid equilibrium, VLE, in the scope of this work), as well as other thermodynamic quantities that arise in the mixing process. These properties are associated with the excess Gibbs energy g^E , which is written as $g^E = g^E(x_i, p, T)$. As such, the goal of the modeling is to achieve a functional type of $f = f(\theta, x_i, p, T)$ that minimizes the norm $|g^E - f|$. The vector θ represents a set of parameters in the model, which must be optimized. However, due to the existing relation between phase and mixing properties, former approach may not be enough. In the first place, g^E values can only be obtained from VLE, which satisfies a dependency of the type, $F(x_i, p, T) = 0$, preventing us from obtaining individual relations of g^E with each one of the variables. On the other hand, defects in the experimental data could give place to incoherencies between experimental activity coefficients $\gamma_i = \gamma_i(x_i, y_i, p, T)$ and the excess Gibbs function g^E . Thus, the VLE fitting process becomes a bi-objective optimization problem; hence, two error functions are included in the correlation problem. The complexity grows as other properties, such as $h^E = h^E(x, p, T)$, are included in the modeling, since new error functions should also be minimized. However, one of the benefits of this approach is to use a unique thermodynamic model that avoids the issues caused by possible discontinuities or inconsistencies between partial models of some properties. Even more relevant is that this allows the model to describe better the physics of the system under study. This supposes a mean to verify the coherence of the mathematical formalism imposed by thermodynamics, validating the different properties. A drawback of this practice is the increase of the complexity of the procedure, but this is just a numerical issue of relative complexity. Therefore, addressing the global modeling of the thermodynamic behavior of solutions as a problem with multiple objectives is a notable contribution in chemical engineering.

It is known that the resolution of multi-objective problems does not produce a single result; on the contrary, a set of non-dominated results that constitute the so-called Pareto front [5] is obtained. There is no precise mathematical criterion that allows the selection of a unique result. However, the process simulation requires a single result to define the intended design, having to resort to external criteria different from those used to obtain the *front*.

This study evaluates the effect of choosing the different results from the *Pareto front* in the simulation task. To achieve this, some partial goals are proposed such as (a) to establish a rigorous methodology to carry out the optimization procedure with the suggested modeling and (b) to check the real impact of the chosen model on the simulation, with the purpose of proposing a selection criterion. Thus, the designed methodology should include different stages, like the data selection used in the procedure, obtaining the *result front* and the election of the final *result*. Two systems, considered as standard in many studies on thermodynamic behavior of solutions, are selected since the necessary experimental information (VLE and h^E) is available in literature. After checking the data sets [6, 7], making up the

testing \leftrightarrow modeling steps, and having obtained the corresponding *result fronts*, each candidate model is analyzed on its suitability for process simulation.

2. Modeling procedures

2.1 Thermodynamic model

The correlation of the iso- p {VLE + h^E } data for each one of the two systems selected is carried out using a parametric equation already used by us [8], which is applied to the excess Gibbs function of a binary system:

$$g^E(p, T, \mathbf{x}) = z_1(1 - z_1) \sum_{i=0}^2 g_i(p, T) z_1^i z_2 = \frac{x_1}{x_1 + k_g^{2-1} x_2} \quad (1)$$

and as described in [8]:

$$g_i(p, T) = g_{i1} + g_{i2} p^2 + g_{i3} p T + g_{i4}/T + g_{i5} T^2 \quad (2)$$

where k_g^{2-1} is a fitting parameter. In this study, several forms of Eq. (2) are tested, by adapting it according to the availability of experimental data. Thus, different “sub-models” are defined by neglecting terms in Eq. (2) which give rise to the following four cases:

$$\begin{aligned} \text{M1} &\rightarrow \{g_{i2}, g_{i3}, g_{i4}, g_{i5}\} = 0; \text{M2} \rightarrow \{g_{i2}, g_{i3}, g_{i5}\} = 0; \\ \text{M3} &\rightarrow \{g_{i2}, g_{i5}\} = 0; \text{M4} \rightarrow g_{i2} = 0 \end{aligned} \quad (3)$$

From Eq. (1), the expression that characterizes the activity coefficients is

$$\begin{aligned} RT \ln \gamma_i &= z_1(1 - z_1)(g_0 + g_1 z_1 + g_2 z_1^2) + (1 - i - x_1) \\ &[g_0 + 2(g_1 - g_0)z_1 + 3(g_2 - g_1)z_1^2 - 4g_2 z_1^3] k_g^{2-1} (z_1/x_1)^2 \end{aligned} \quad (4)$$

Likewise, the excess enthalpies h^E are calculated considering.

$$h^E = g^E - T(\partial g^E / \partial T)_{x,p}; h^E = z_1(1 - z_1)(h_0 + h_1 z_1 + h_2 z_1^2) \quad (5)$$

Eqs. (1) and (5) assume that the different sub-models established by Eq. (3) impose certain behavior hypothesis in the mixture. Thus, sub-model M1 implies that $g^E = h^E$. For the remaining assumptions, $g^E \neq h^E$, allowing different functions to express the h^E s.

2.2 Calculation of the *efficient fronts*

To obtain the optimal parameters of the different sub-models that represent the data set iso- p VLE and h^E , the multi-objective optimization (MOO) procedure is used, which is characterized by the vector

$$\mathbf{OF} = [s(g^E/RT) \quad s(h^E)] \quad (6)$$

where $s(y^E)$ is the root of the mean square error (or RMSE) calculated by the model when representing the generic property y^E :

$$s(y^E) = \left[\sum (y_{\text{exp}}^E - y_{\text{cal}}^E)^2 / m \right]^{0.5}; m = \text{number of experimental points} \quad (7)$$

The result of such a problem is a discrete set of values, taken from the *efficient front*, $s(g^E/RT) = f[s(h^E)]$, where each one of these give rise to different estimates of the thermodynamic behavior. Here the ε -constraint algorithm [3] is used to solve the MOO optimization problem. This procedure converts the multi-objective nonlinear problem (MNLP) into multiple single-objective problem (constrained nonlinear problem (CNLP)), thence minimizing only the first objective in Eq. (6), that is,

$$OF_\varepsilon = s(g^E/RT) \quad (8)$$

using the other vector element to establish a constraint in the calculation, that is,

$$\text{constraint} \rightarrow s(h^E) < \varepsilon \quad (9)$$

The value of ε is limited, from 0 to 500 J mol⁻¹, since greater errors in the h^E are not acceptable. The *efficient front* is then achieved by solving the CNLP (Eqs. (8) and (9)) for different values of ε in the indicated range. To do so, we used a hybrid evolutionary algorithm [3], coupled with Nelder-Mead algorithm [9], for local refinement.

3. Verification and selection of data series

3.1 Acetone + ethanol

There are 10 useful references in literature containing VLE data for the acetone(1) + ethanol(2) system [10–19] showing a total of 15 experimental series. In **Figure 1**, seven sets are iso- p (**Figure 1(a)**), and eight sets are iso- T (**Figure 1(b)**).

For use we refer to data series with information for the two phases. This is a requirement to check the thermodynamic consistency. **Figure 1(b)** shows an azeotrope at high pressures, which moves from the acetone-rich region toward pure ethanol as pressure increases; the separation between the compositions in the two phases is reduced. **Figure 1(c)** and **(d)** contains, respectively, the variation of γ_1 and g^E/RT with the liquid composition for the system at 101 kPa. Ethanol's activity coefficient shows some errors that surely affect the global consistency of the data series. High slopes are observed as $x_1 \rightarrow 0$ along with negative values of the natural logarithm of γ_1 for data series other than those referenced [14–16]. This is a clear sign of inconsistency.

Table 1 shows the results obtained in the application of different consistency methods. The observation of the said table produces some comments which are interesting in the work development. The Wisniak test and the direct van Ness test accept most of the experimental series. The first of the methods rejects two (noted as n° 10,12) while the second fails to validate only one, n° 8. The Kojima test rejects five data series, with the error observed in the system n° 12 being critical. A new methodology recently proposed by us [6, 7] was also applied, which rejects nine systems: three by the *integral form* (n° 9, 11, 12) and six by the *differential form* (n° 1, 3, 4, 8, 9, 12). These systems present obvious signs of inconsistency that are also observed by at least one of the other methods. Therefore, the overall assessment of these series (in other words, the quality of their experimental data) is not

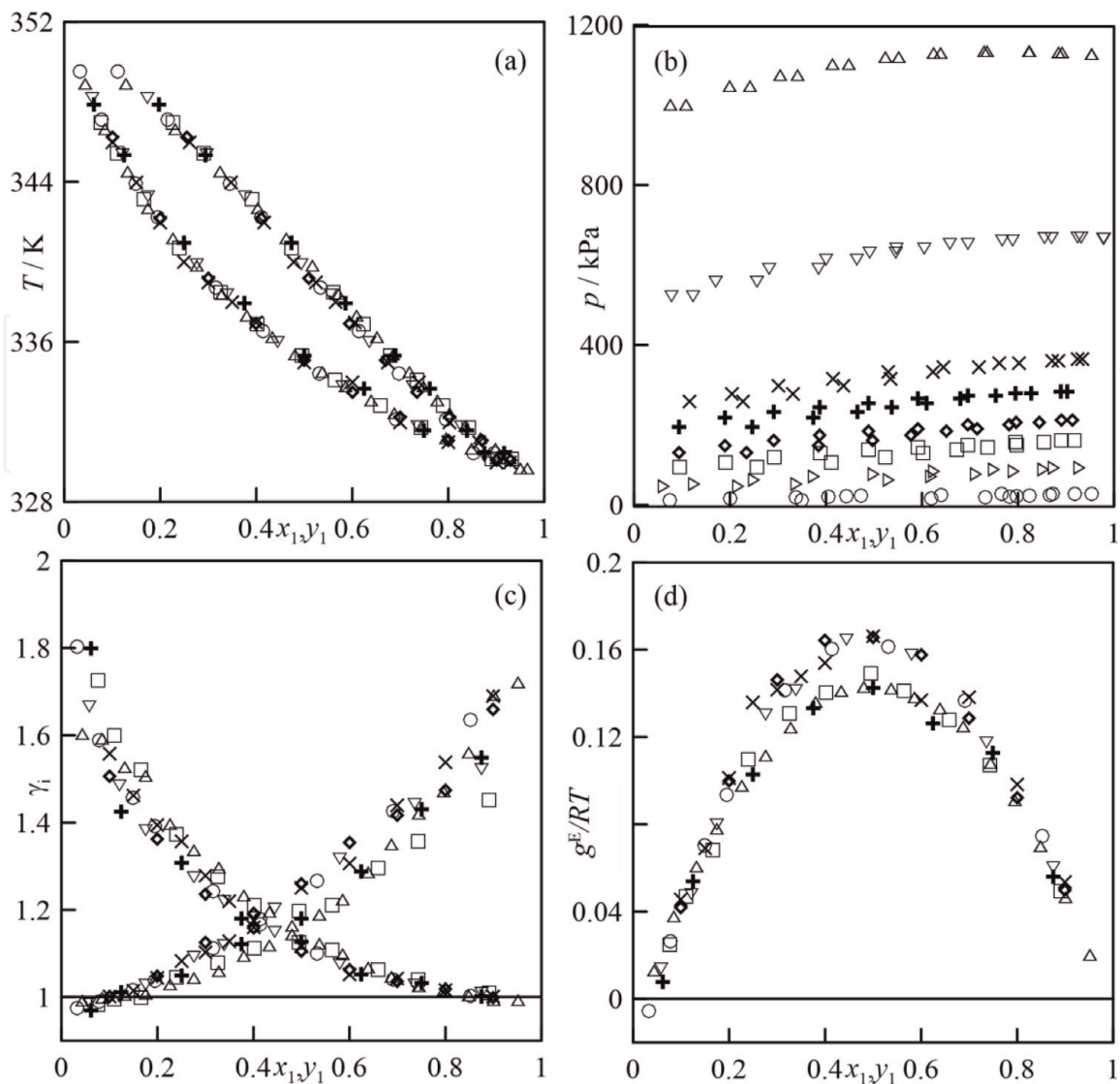


Figure 1. Plot of VLE data of the binary: acetone(1) + ethanol(2), *iso-p* ≈ 101.32 kPa. (a) T, x, y ; (c) γ, x ; (d) $g^E/RT, x$. (\times) Ref. [10]; (∇) Ref. [11]; (\circ) Ref. [12]; (\diamond) Ref. [13]; (+) Ref. [14]; (\triangle) Ref. [15]; (\square) Ref. [16]; (b) p, x, y . *iso-T*: (\triangleright) Ref. [14]; (\circ) Ref. [17]; Ref. [18] (\times) $T = 372.67$ K; (∇) $T = 422.56$ K, (\triangle) $T = 397.67$ K; Ref. [19], (\square) $T = 344.19$ K, (+) $T = 363.19$ K, (\diamond) $T = 358.18$ K.

positive, ruling out the use of these series for other subsequent tasks, such as modeling and, specially, simulation.

Regarding h^E , six references were found [20–25]. All extracted values are shown in **Figure 2(a and b)**, where the different series show an acceptable coherence, having $(dh^E/dT)_{p,x} > 0$.

3.2 Benzene + hexane

In studies related to the thermodynamics of solutions, the experimental information generated by the binary benzene + hexane, for different properties, has been, and still is, used by researchers in that area as a reference of their investigations; therefore, the choice of this system is justified. Twenty-three useful VLE data series were found in the bibliography [26–42], 16 *iso-p* and 7 *iso-T*. **Figure 3** shows important errors in some of the series [29, 31, 37] at 101 kPa, with data missing the trend observed in the other series. These are propagated to the T vs x, y representations (**Figure 4(a)**). The random error for these series is serious as evidenced in **Figure 4(b)**.

N°	Ref.	Type	Area	Fredenslund		Wisniak		Kojima		Direct-Van Ness		Proposed test					
				$d\%$	V	$\times 100$	V	D_w	V	$M(I_i)$	V	$\delta \ln(\gamma_1/\gamma_2)$	V	$f-int.$	V	$f-dif.$	V
1	10	Iso-101 kPa	15	nv	1.9	nv	2.5	v	24	v	0.09	v	0.06	v	-0.06	nv	nv
2	11	Iso-101 kPa	13	nv	1.8	nv	2.6	v	18	v	0.09	v	0	v	0.004	v	v
3	12	Iso-101 kPa	15	nv	1.8	nv	1.7	v	10	v	0.09	v	0.14	v	-0.05	nv	nv
4	13	Iso-101 kPa	23	nv	2.2	nv	2	v	15	v	0.09	v	0.11	v	-0.08	nv	nv
5	14	Iso-101 kPa	5	nv	1.2	nv	0.5	v	27	v	0.04	v	0	v	0.003	v	v
6	15	Iso-101 kPa	7.1	nv	0.5	v	2.1	v	16	v	0.02	v	0.16	v	0.005	v	v
7	16	Iso-101 kPa	1.4	v	0.6	v	2.8	v	40	nv	0	v	0.02	v	0.006	v	v
8	14	Iso-328 K	1.7	v	0.9	v	2.1	v	74	nv	0.01	v	0.36	v	-0.050	nv	nv
9	17	Iso-298 K	41	nv	2.7	nv	1.5	v	82	nv	0.18	nv	-0.09	nv	-0.370	nv	nv
10	18	Iso-372 K	3.3	nv	0.4	v	3.3	nv	14	v	0.02	v	0.11	v	0.009	v	v
11	18	Iso-398 K	0.4	v	0.6	v	3	v	69	nv	0.02	v	-2	nv	0.001	v	nv
12	18	Iso-423 K	12	nv	0.6	v	4.4	nv	159	nv	0.01	v	-24.5	nv	-0.01	nv	nv
13	19	Iso-344 K	2.8	nv	0.3	v	2.1	v	14	v	0.01	v	0.42	v	0.016	v	v
14	19	Iso-358 K	3.3	nv	0.3	v	3	v	9	v	0.01	v	0.64	v	0.014	v	v
15	19	Iso-363 K	0.2	v	0.2	v	2.5	v	19	v	0.01	v	0.83	v	0.029	v	v

Limiting values: areas-test: $d < 2$; Fredenslund-test: $\delta y \times 100 < 1$; Wisniak-test: $D_w < 3$; Kojima-test: $M(I_i) < 30$; Direct Van Ness-test: $\delta(\ln \gamma_1 / \ln \gamma_2) < 0.16$; proposed-test: $f-int > 0$, $f-dif > 0$. Header notation: V \rightarrow verified; FV \rightarrow fully verified. Test outcome: v \rightarrow verified; nv \rightarrow not verified; nd/- \rightarrow not available.

Table 1.

Values obtained in the application of the thermodynamic consistency-test to VLE data of acetone + ethanol at different conditions.

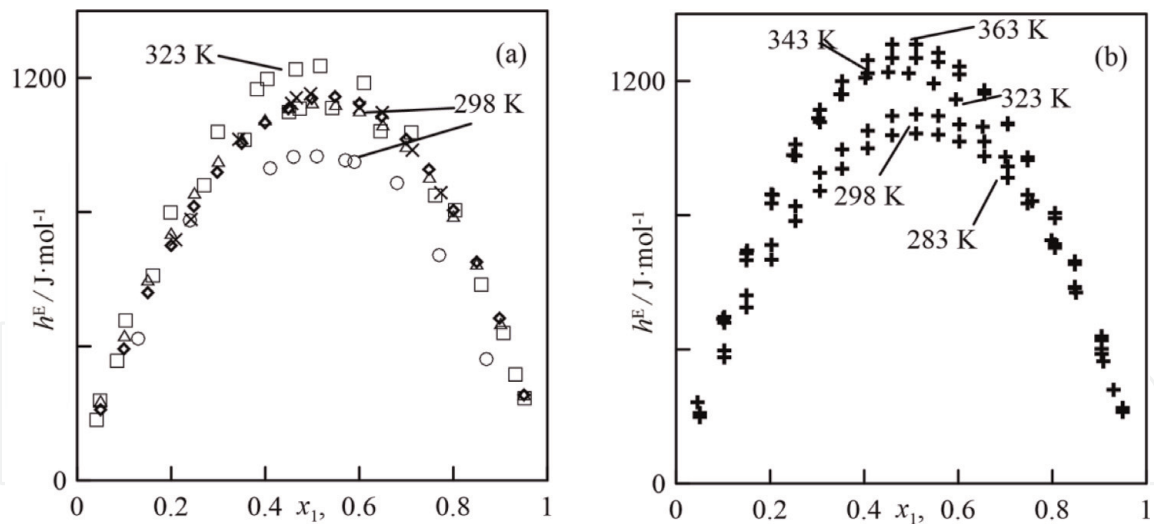


Figure 2.
 h^E values for the binary acetone(1) + ethanol(2). (a) $p = 101.32$ kPa; (b) $p = 400$ kPa. (O) Ref. [20]; (X) Ref. [21]; (□) Ref. [22]; (+) Ref. [23]; (△) Ref. [24]; (◇) Ref. [25].

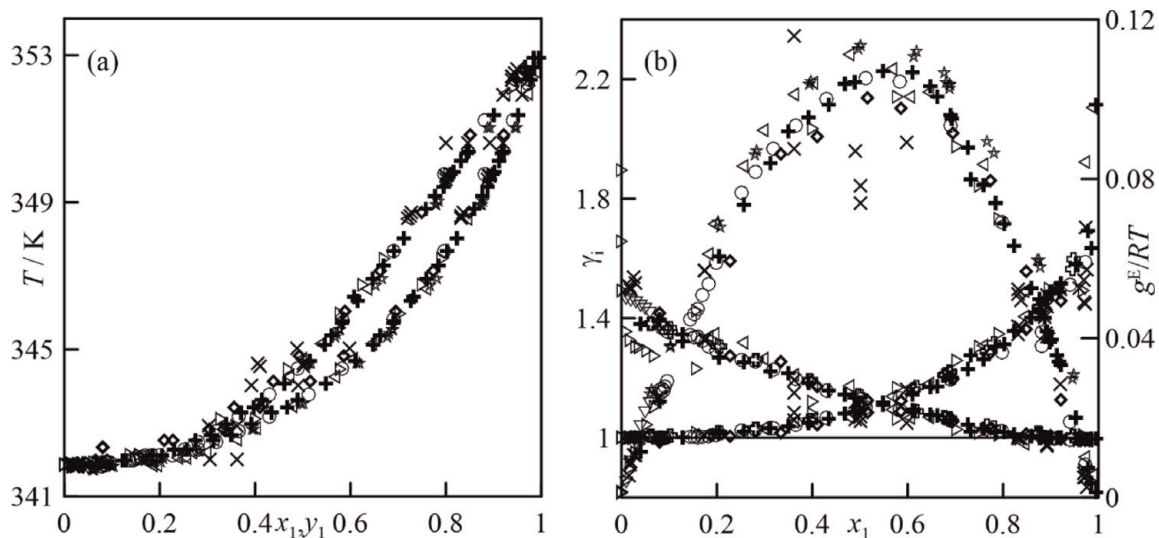
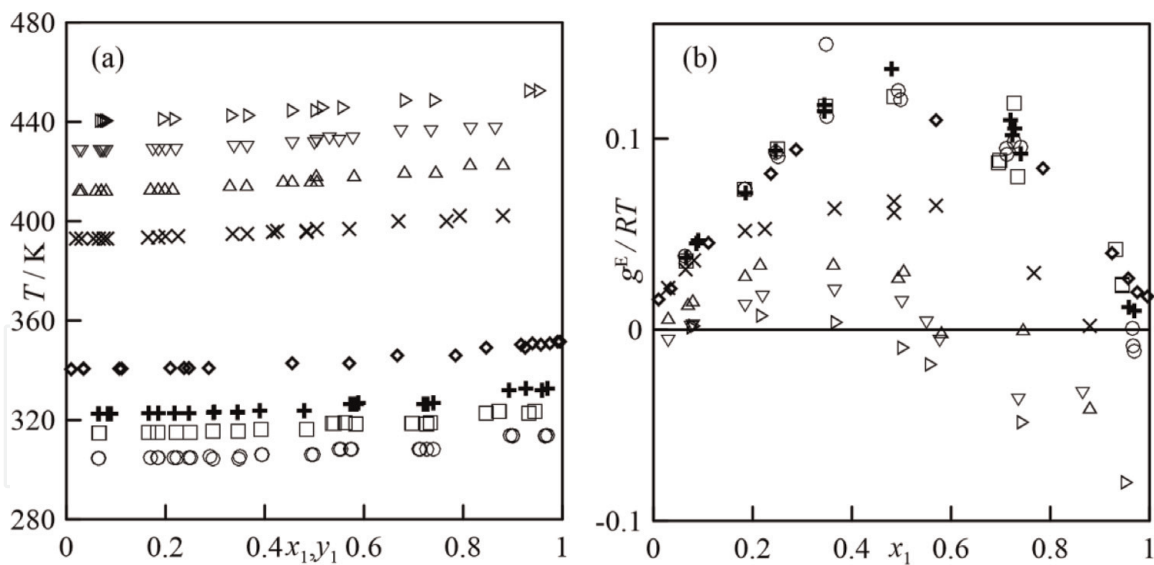


Figure 3.
 Plot of iso- p VLE data of the binary benzene + hexane at 101 kPa. (a) T, x, y ; (b) $\gamma_i, x; g^E/RT, x$. (O) Ref. [34] (★) Ref. [35] (+) Ref. [26] (◇) Ref. [37]; (X) Ref. [29]; (▽) Ref. [32]; (▷) Ref. [31]; (◁) Ref. [37].

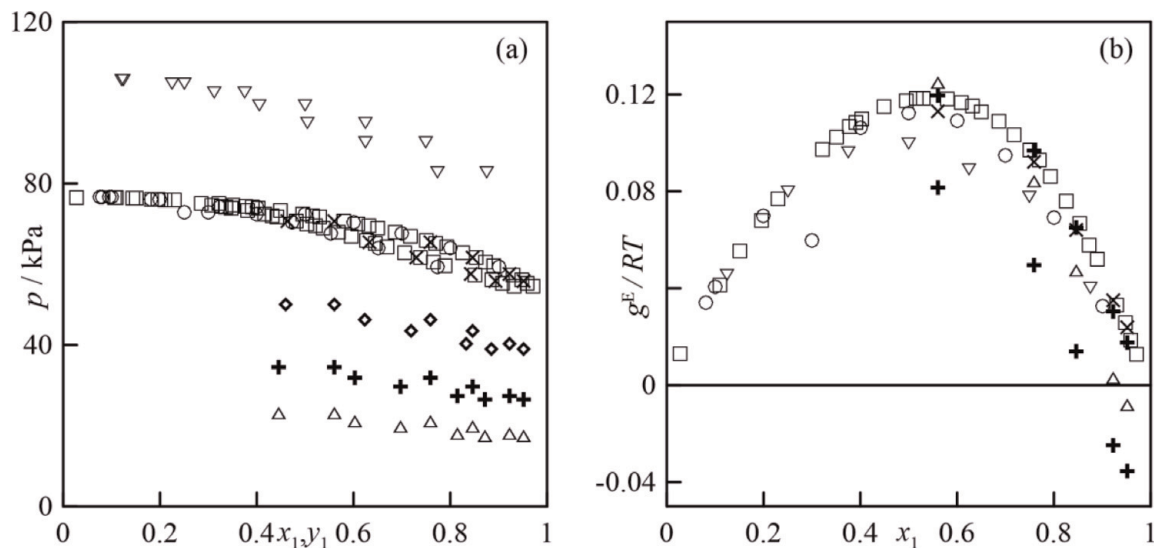
Figure 4 depicts the iso- p data set at pressures other than the atmospheric. **Figure 5(b)** indicates that three of the published series [28] (the ones that correspond to $p = 610.8$ kPa, 810.8 kPa, and 1013.5 kPa) show systematic errors, giving rise to $g^E/RT < 0$; thus $\gamma_i < 1$ as $x_1 \rightarrow 1$. However, the representation of T vs x, y does not reflect this anomalous behavior, so that probably they will be caused by a systematic deficiency in the monitored temperature.

Available iso- T data series are represented in **Figure 5**. Data are found for the whole composition interval only at 333 and 345 K. Several series were measured at 333 K [40–42], allowing their comparison. From the representation of p, x, y (**Figure 5(a)**) and related mixing quantities (**Figure 5(b)**), an acceptable coincidence is observed. Two of the data sets (Ref. [41]) show negative values of g^E/RT in the extreme points, at infinite dilution, which is a clear sign of inconsistency.

Conclusions drawn from the visual inspection are confirmed by the consistency analysis presented in **Table 2**. Data series n° 11 is discarded since consistency cannot be evaluated due to the lack of data in the zone corresponding to $x_1 > 0.2$. All consistency tests, except the direct van Ness, did not accept the series measured at


Figure 4.

Plot of iso- p VLE of the binary benzene(1) + hexane(2). (a) T, x, y ; (b) $g^E/RT, x$. Ref. [33]: (○) $p = 26$ kPa; (□) $p = 40$ kPa; (+) $p = 53$ kPa; (◇) Ref. [26]; Ref. [28]: (×) $p = 405.4$ kPa; (△) $p = 610.8$ kPa; (▽) $p = 810.8$ kPa; (▷) $p = 1013.5$ kPa.


Figure 5.

Plot of iso- T VLE data of the binary benzene(1) + hexane(2). (a) p, x, y ; (b) $g^E/RT, x$. (○) Ref. [40]; (□) Ref. [42] Ref. [41]: (+) $T = 314$ K; (◇) $T = 323$ K; (×) $T = 333$ K; (△) $T = 303$ K; (▽) Ref. [39].

the highest pressures (n° 13–16). This is due to the wrong relationship between the pure component saturation temperature (Appendix **Table A1**) and equilibrium temperature. However, it is interesting to recognize that when using other vapor pressure parameters this defect can be solved. The data series (n° 3, 4, 6–9, 19, 21–23) accepted by the proposed test [7] offer the highest consensus among all the battery of test about the quality of data, so these series could be used for subsequent tasks.

A total of 17 references were found in literature [36, 43–58] of h^E measured in the range of [293–323] K and atmospheric pressure, except those data of Yi et al. [58], at 80 kPa. **Figure 6(a)** presents the data series considered in this study. It refers to a solution with endothermic effects ($h^E \approx 900$ J mol⁻¹ at $x = 0.5$ and $T = 298$ K), decreasing as temperature increases; however, the high observed dispersion of experimental values is not sufficient evidence to ensure this effect. Inspection of the h^E does not recommend excluding any of these data series; thus they will be considered in the data treatment.

N°	Ref.	Type	Area	Fredenslund		Wisniak		Kojima		Direct-Van Ness		Proposed test					
				d%	V	$\times 100$	V	D_w	V	$M(I_i)$	V	$\delta \ln(\gamma_1/\gamma_2)$	V	<i>f-int.</i>	V	<i>f-dif.</i>	V
1	33	Iso-26 kPa	23.2	nv	1.2	nv	1.45	v	74	nv	0.123	v	-0.06	nv	-0.073	nv	nv
2	33	Iso-40 kPa	16.3	nv	1.2	nv	1.02	v	19	v	0.068	v	-0.02	nv	-0.013	nv	nv
3	33	Iso-53 kPa	17.5	nv	0.8	v	1.93	v	31	nv	0.063	v	0.04	v	0.001	v	v
4	26	Iso-97 kPa	19.2	nv	0.6	v	1.7	v	54	nv	0.02	v	0.05	v	0.005	v	v
5	31	Iso-101 kPa	36.5	nv	0.6	v	1.65	v	10	v	0.012	v	0.02	v	-0.047	nv	nv
6	26	Iso-101 kPa	3.6	nv	0.4	v	1.6	v	24	v	0.020	v	0.11	v	0.006	v	v
7	34	Iso-101 kPa	2.5	nv	0.3	v	1.63	v	24	v	0.004	v	0.04	v	0.007	v	v
8	35	Iso-101 kPa	1.5	v	0.1	v	1.7	v	27	v	0.003	v	0.01	v	0.014	v	v
9	37	iso-101 kPa	9	nv	0.4	v	1.75	v	44	nv	0.159	v	0.05	v	0.004	v	v
10	29	iso-101 kPa	12.3	nv	0.6	v	1.66	v	22	v	0.048	v	-0.01	nv	-0.013	nv	nv
11	32	Iso-101 kPa	nd	—	nd	—	nd	—	nd	—	nd	—	nd	—	nd	—	nv
12	37	Iso-101 kPa	9	nv	0.7	v	2.77	v	52	nv	0.043	v	0.02	v	-0.018	nv	nv
13	28	Iso-405 kPa	59	nv	1.2	nv	5.9	nv	1319	nv	0.2	nv	-0.21	nv	-0.145	nv	nv
14	28	Iso-610 kPa	58.9	nv	1.1	nv	7.51	nv	343	nv	0.043	v	-0.14	nv	-0.079	nv	nv
15	28	Iso-810 kPa	96.3	nv	2	nv	11.5	nv	291	nv	0.124	v	-0.16	nv	-0.08	nv	nv
16	28	Iso-1010 kPa	95.4	nv	3	nv	14.97	nv	6776	nv	0.364	nv	-0.07	nv	-0.192	nv	nv
17	41	Iso-303 K	16.8	nv	1.6	nv	0.61	v	670	nv	0.167	nv	0.03	v	-0.096	nv	nv
18	41	Iso-314 K	17.5	nv	2.7	nv	0.68	v	1149	nv	0.312	nv	0	nv	-0.122	nv	nv
19	41	Iso-323 K	7.9	nv	0.6	v	0.97	v	270	nv	0.048	v	0.13	v	0.006	v	v
20	40	Iso-333 K	31.1	nv	1.8	nv	2.42	v	41	nv	0.082	v	-0.33	nv	-0.048	nv	nv

N°	Ref.	Type	Area	Fredenslund		Wisniak		Kojima		Direct-Van Ness		Proposed test					
				d%	V	$\times 100$	V	D_w	V	$M(I_i)$	V	$\delta \ln(\gamma_1/\gamma_2)$	V	<i>f-int.</i>	V	<i>f-dif.</i>	V
21	42	Iso-333 K	1.7	v	0.1	v	1.31	v	12	v	0.002	v	0.5	v	0.017	v	v
22	41	Iso-333 K	1.2	v	0.4	v	1.22	v	88	nv	0.017	v	0.41	v	0.009	v	v
23	39	Iso-343 K	7.4	nv	0.5	v	1.53	v	19	v	0.027	v	0.29	v	0.001	v	v

Limiting values: areas-test: $d < 2$; Fredenslund-test: $\delta y \times 100 < 1$; Wisniak-test: $D_w < 3$; Kojima-test: $M(I_i) < 30$; direct Van Ness-test: $\delta(\ln \gamma_1/\ln \gamma_2) < 0.16$; proposed-test: $f\text{-int} > 0$, $f\text{-dif} > 0$. Header notation: V \rightarrow verified; FV \rightarrow fully verified. Test outcome: v \rightarrow verified; nv \rightarrow not verified; nd/- \rightarrow not available.

Table 2.

Values obtained in the application of the thermodynamic consistency-test to VLE data of benzene + hexane at different conditions.

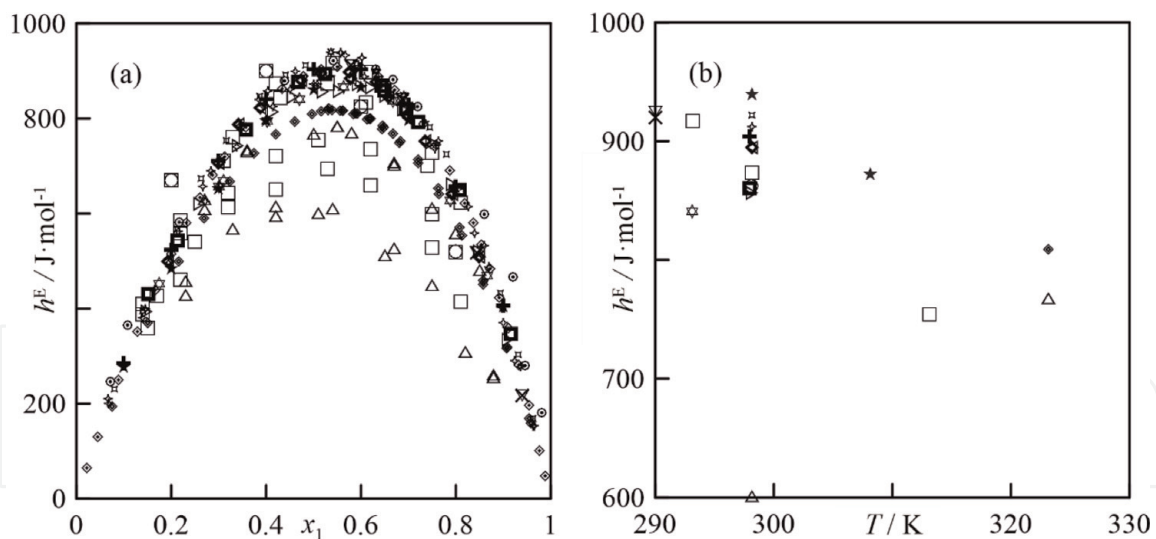


Figure 6. Plot of h^E values for the binary benzene + hexane. (a) h^E vs x , (b) h^E (at $x = 0.5$) vs T . (\circ) Ref. [43], (\square) Ref. [44], ($+$) Ref. [45], (\diamond) Ref. [46], (\times) Ref. [47], (\triangle) Ref. [48], (∇) Ref. [36], (\triangleright) Ref. [49], (\triangleleft) Ref. [50], (\square) Ref. [51], (\blacksquare) Ref. [52], (\diamond) Ref. [53], (\boxtimes) Ref. [54], (\odot) Ref. [55], (\star) Ref. [56], (\blacklozenge) Ref. [57], (\blacklozenge) Ref. [58].

4. Results and discussion

4.1 Modeling: efficient front and models

The VLE data series previously verified has been modeled according to the procedure described in Section 2. The *efficient fronts* obtained for each system are shown in Figure 7.

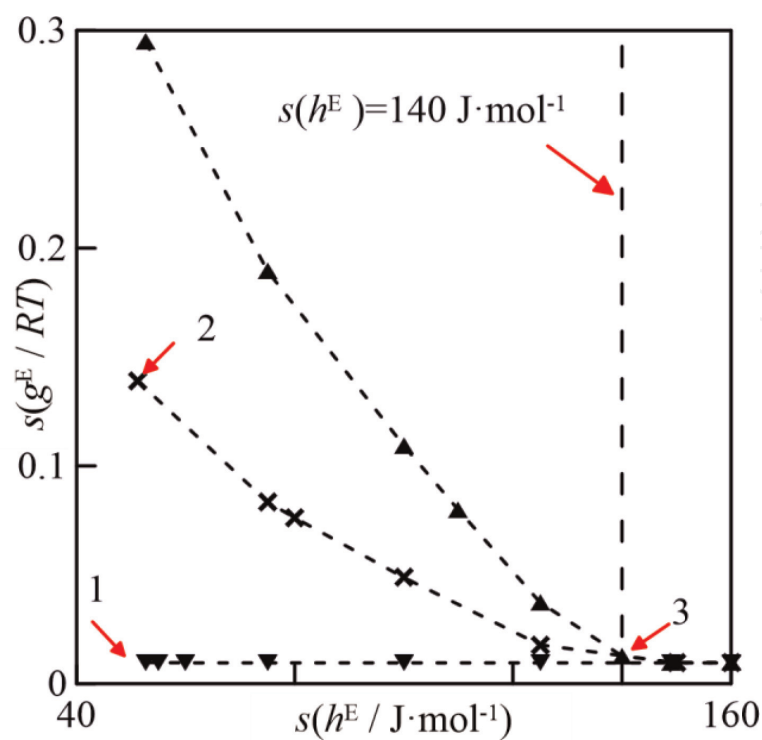


Figure 7. Efficient fronts for $s(g^E/RT) = f(s(h^E))$, obtained for acetone + ethanol. Arrows and labels indicate the chosen results on each of the fronts, using the models: (\blacktriangle) M2; (\times) M3; and (\blacktriangledown) M4.

Acetone(1) + ethanol(2): the efficient fronts of results for the binary acetone + ethanol were obtained from sub-models M2, M3, and M4. Sub-model M1 did not produce an acceptable representation of the thermodynamic behavior, so it was ignored. The obtained fronts shown in **Figure 7** reveal that the three sub-models produced similar results when acceptable error in h^E is greater than 140 J mol^{-1} . This implies that, from this limit on, the problem becomes mono-objective, regardless of the sub-model used. For smaller errors of the h^E , $s(h^E) < 140 \text{ J mol}^{-1}$, differences between sub-models M2, M3, and M4 to reproduce the VLE data are significant, reducing the maximum error by approximately $\delta s(g^E/RT) \approx 0.15$ between them. The *efficient front* achieved with model M4 shows an almost constant $s(g^E/RT)$. The other two sub-models reveal an exponential behavior as $s(h^E)$ decreases. From the set of results obtained, three of them are chosen (see **Figure 7**) to carry out a more detailed analysis on their ability to describe simultaneously the VLE and h^E . Some particular comments on those *three results* are:

- The *result* labeled as “1” (by M4) describes well the two properties under study, as seen in **Figure 8**, but at the expense of using more parameters. Specifically, this model links the state variables at equilibrium (**Figure 8(a)**), describing the observed folding at the lowest temperatures. The estimate of

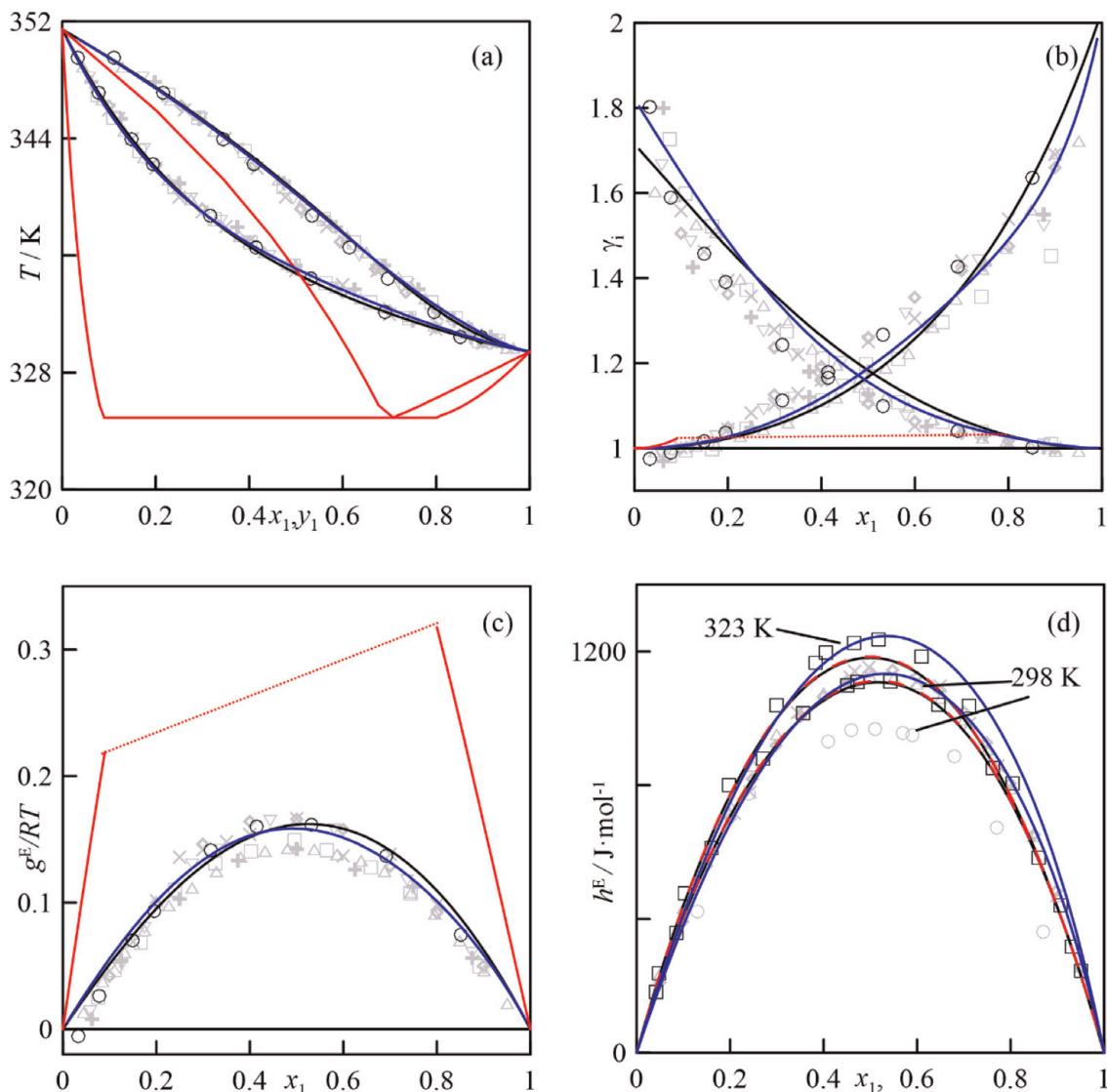


Figure 8.

Plot of VLE at 101 kPa and h^E estimates for binary acetone(1) + ethanol(2) at 101.32 kPa. Models drawn from **Figure 7(a)**. Results (—) 1-(M4), (—) 2-(M3), (—) 3-(M3). (a) T vs x_1, y_1 ; (b) γ_i vs x_1 ; (c) g^E/RT vs x_1 ; (d) h^E vs x_1 .

activity coefficients (**Figure 8(b)**) is acceptable. Estimations of g^E/RT for this system are close to the set that displays the highest values. The estimate for the h^E is acceptable, although the model does not reproduce the data series extracted from Ref. [20].

- *Result 2* (M3), which displays the highest error in the VLE estimate, wrongly estimates an azeotrope and a whole range immiscible region (**Figure 8(a)**). This poor description of the liquid phase is due to the high values of γ_i and the g^E/RT (**Figure 8(b and c)**). At first, the h^E is correctly represented by this parametrization, although the presence of the immiscibility truncates the validity region of the model (**Figure 8(d)**).
- *Result 3* (M3) produces an unsatisfactory representation in the h^E s, which also presents an inversion of the thermal gradient of this property.

Final model selection should ensure that selected parametrization describes, at least qualitatively, the thermodynamic behavior closest to the real one. In this case, *result 2* reproduces almost exactly the h^E , although it produces an incorrect g^E behavior, hence limiting its subsequent applicability. The choice between *results 1* and *3* will depend on the influence of the h^E on the calculations in which the model is involved.

This analysis will serve as a basis to inspect the results of the remaining binary (benzene + hexane) on the results emitted by each of the models.

Benzene(1) + hexane(2): sub-model M4 was not used for the binary benzene + hexane because of the similarity with the *efficient front* produced by M3 model. Thus, sub-models M1, M2, and M3 were only applied, as shown in **Figure 9**. Sub-models M2 and M3 produce very similar results, with almost constant error, $s(g^E/RT)$, lower than $5.5 \times 10^{-3} \text{ J mol}^{-1}$ for all $s(h^E)$. Consequently, those *result fronts* of sub-models M1 and M2 are evaluated. The *efficient front* of sub-model M1

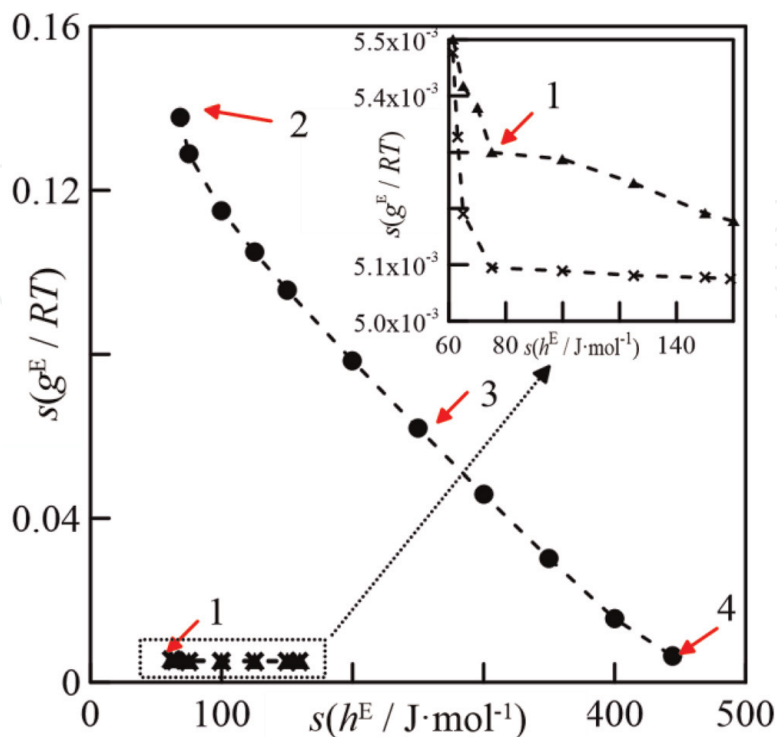


Figure 9. Efficient fronts for $s(g^E/RT) = f(s(h^E))$, obtained for benzene + hexane. Arrows and labels indicate the chosen results on each of the fronts, using the models: (●) M1; (▲) M2; and (×) M3.

produces a quasi-linear behavior with the variation of $s(h^E)$. The difference between this *front* and that of sub-model M2 is $\delta s(g^E/RT) \approx 0.14$, when $\varepsilon = 0$. The *fronts* for models M1 and M2 do not intersect, unlike the earlier case, showing a maximum value of $s(h^E)$ at 170 J mol^{-1} and 450 J mol^{-1} , respectively. The VLE diagrams produced by the *four selected results* are shown in **Figure 10**, along with one of the validated data series for this *result*. The best description of this system is achieved with *result 4* (M1), which reproduces the behavior of T - x - y experimental data (**Figure 10(a)**) and the other quantities calculated (**Figure 10(b and c)**). Nevertheless, the description of h^E with this model is not good. *Result 1* (M2) produces an azeotrope at $x_1 < 0.2$, which does not occur experimentally. This poor estimation occurs even though the greater number of parameters, increasing the model's capacity to reproduce the h^E , as proven in **Figure 11**. *Results 2 and 3* overestimate γ_i , hence g^E/RT (see **Figure 10(b and c)**).

This discrepancy gives rise to the formation of minimum boiling point azeotropes, which are not in accordance with experimental data. Of all the *results* chosen, only *result 1* (belonging to sub-model M2) shows a h^E that varies significantly with temperature, since sub-model M1 is independent of this variable. The use of either *result 2* or *3* is discouraged since their estimations of h^E , especially at temperatures other than 298 K, are not correct, in addition to the described issues in

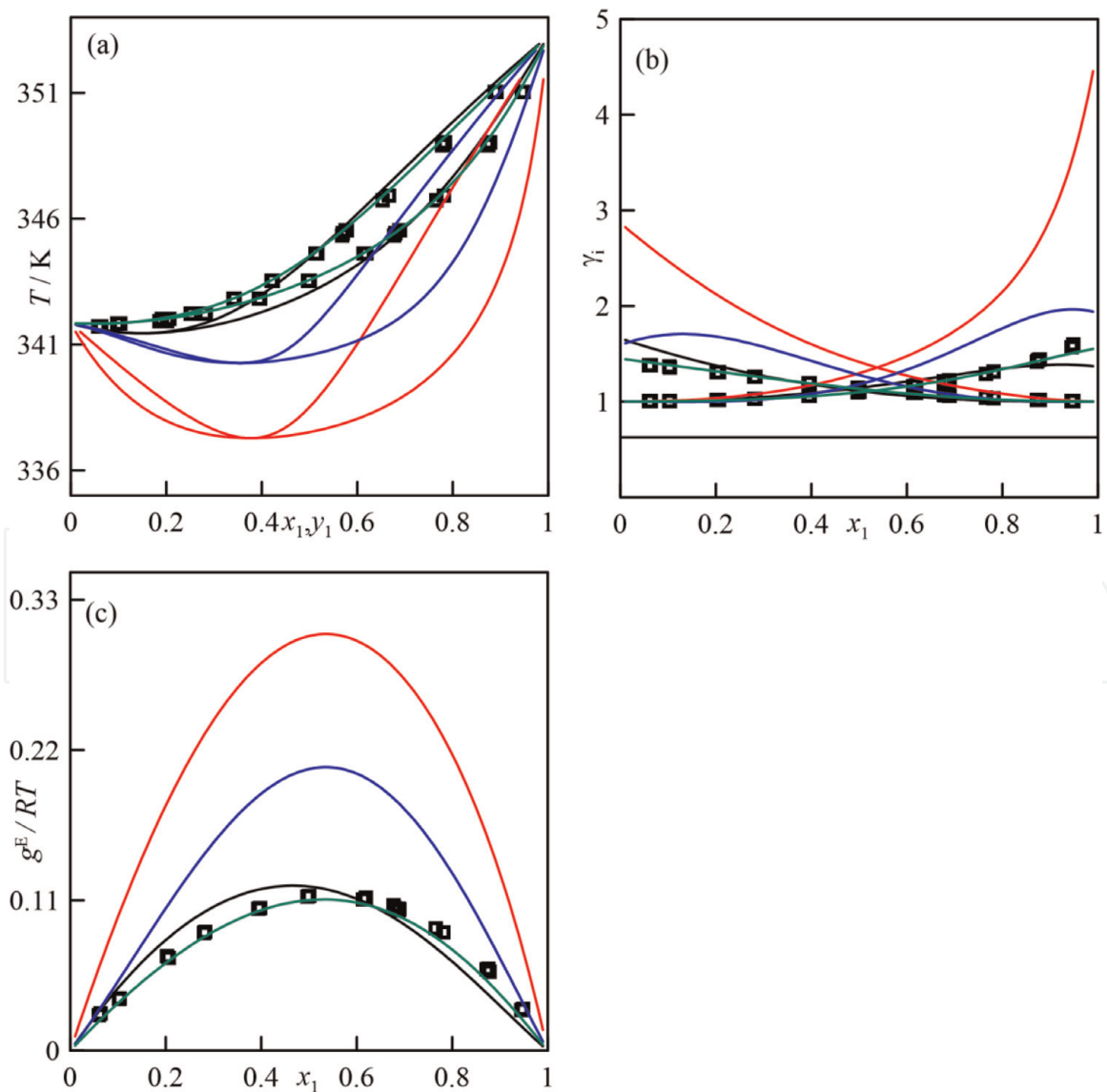


Figure 10.

Plot of VLE at 101 kPa estimates for binary benzene(1) + hexane(2). Models drawn from **Figure 9**. Results (—) 1 (M2), (—) 2 (M1), (—) 3 (M1) and 4 (—) (M1). (a) T vs x,y ; (b) γ vs x ; (c) g^E/RT vs x .

representing the phase equilibria. This being said, *result 3* represents the average behavior of this property in the working range.

From previous observations, *result 4* (M1) is recommended for those cases where the h^E plays a secondary role in comparison to the reliable reproduction of the VLE diagram. Otherwise, *result 1* (M2) is preferred, despite the qualitative misfit to experimental data. **Table 3** presents an overview of the present section with a summary of the models to be used in the simulation task.

4.2 Simulation results of a rectification process for each of the studied dissolutions

The models obtained previously are used in the design of a simulation operation comparing their capacity in terms of some operation variables such as composition and temperature profiles, as well as energy consumption. General conditions for the simulations are summarized in **Table 4**. In all cases, columns are fed with a 1 kmol/h at equimolar composition of the corresponding solution, at 298.15 K and 101.32 kPa. Simulations are performed using the RadFrac block of AspenPlus[®] V8.8 (AspenOne[®], [59]).

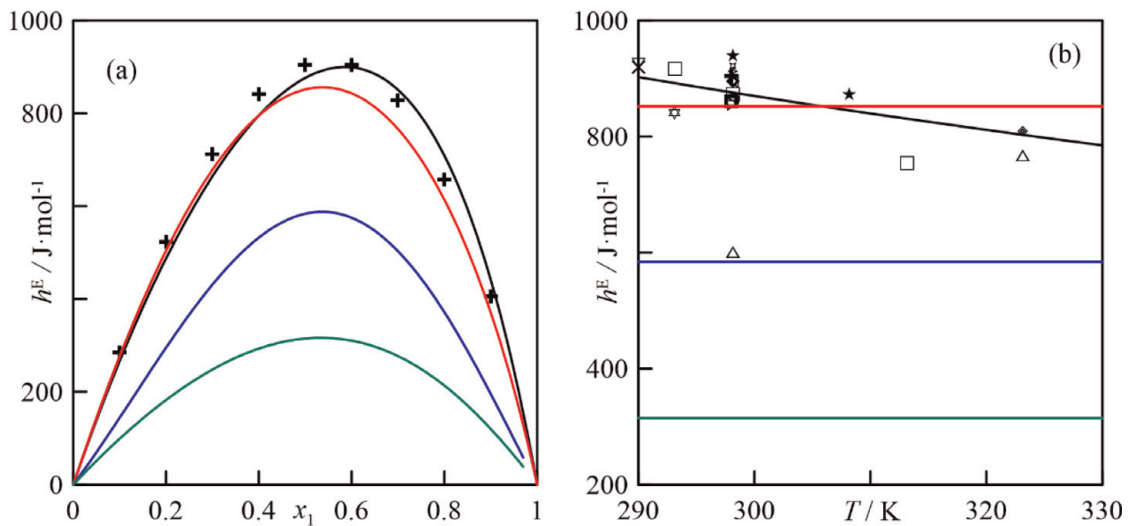


Figure 11. Estimation of h^E values at 101.32 kPa using the different results indicated in the fronts of **Figure 9** for benzene (1) + hexane (2). (a) h^E vs x_1 ($T = 298.15 \text{ K}$), (b) h^E vs T ($x_1 = 0.5$). Results (—) 1 (M2); (—) 2 (M1); (—) 3 (M1); (—) 4 (M1).

System	M1	M2	M3	M4
Acetone + ethanol	✗	✓	✓✓	✓✓
Benzene + hexane	✓✓	✓✓	✓	✗

✓✓ → used for modeling and simulation; ✓ → used for modeling; ✗ → not used.

Table 3. List of sub-models applied to each system.

Binary system	Reflux ratio	Distillate rate (kmol/h)	n° stages	Feed stage
Acetone + ethanol	6	0.5	22	16
Benzene + hexane	10	0.6	30	20

Table 4. Operation data for the rectification columns to separate the binaries.

Acetone(1) + ethanol(2): the simulation of a rectification column to purify the acetone+ethanol binary system, using the *result* labeled as “2” in **Figure 7**, does not provide a coherent resolution because it estimates the presence of two immiscible liquid phases. The final values obtained with *results* 1 and 3 are detailed in **Table 5**, while the composition profiles are shown in **Figure 12**. In both cases the composition of the distillate is higher than 99% in acetone and at the same temperature in the stage.

The exact purity is slightly higher with *result* 1 than with *result* 3, the difference being 0.2%. The calculation in the bottoms of the tower reveals differences between the two parametrizations, giving place to an effluent somewhat purer in the case of *result* 1. The difference between both models is 0.001 in molar fraction. These observations directly affect the calculation of the energy balance and, therefore, to the consumed energy. Thus, the consumption in the condenser is estimated similarly with both parametrizations, while that of the reboiler is significantly higher with *result* 3, due to the greater quantity of ethanol and the incorrect estimate of other quantities, such as the mixing enthalpies.

Stage	Result 1 (M4)			Result 3 (M3)		
	x_1	y_1	T/K	x_1	y_1	T/K
1	0.990	0.993	329.0	0.989	0.991	329.0
5	0.974	0.981	329.1	0.970	0.978	329.1
9	0.941	0.957	329.3	0.935	0.953	329.4
13	0.853	0.900	330.1	0.846	0.894	330.2
17	0.518	0.709	334.4	0.526	0.710	334.2
22	0.010	0.031	350.6	0.011	0.035	350.5
$Q_c/kJ h^{-1}$		1.035E5			1.034E5	
$Q_r/kJ h^{-1}$		1.038E5			1.044E5	

Table 5.

Quantities obtained in the simulation of a separation process for the binary acetone(1) + ethanol(2), using different values from the efficient front shown in **Figure 7**.

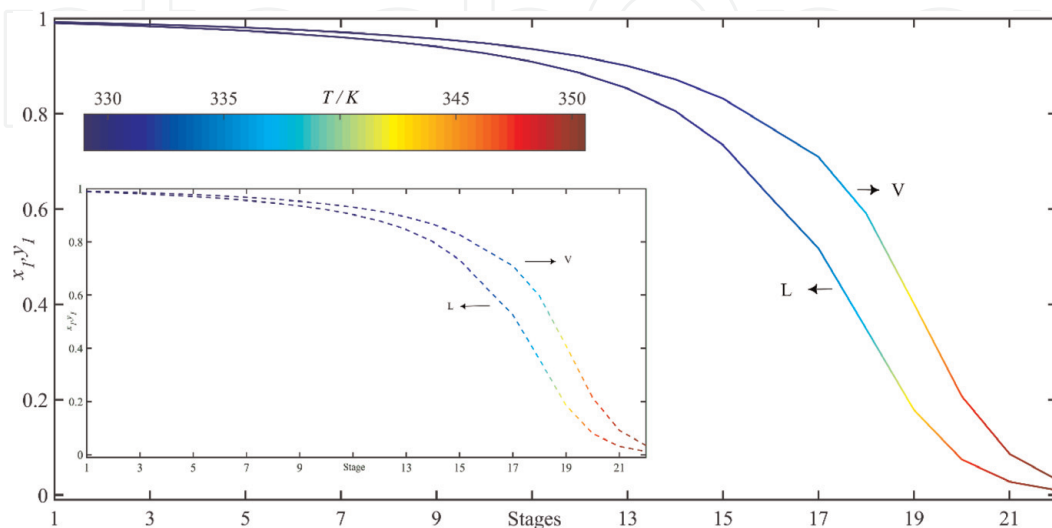


Figure 12.

Plot of composition and temperature profiles obtained in the simulation of a separation operation for acetone (1) + ethanol(2) system, using the different parametrizations proposed: (—) 1 (M4). L, liquid stream profile; V, vapor stream profile.

The composition profiles and temperature gradient of the two tested solutions present similar qualitative behaviors. Most of the column is used as an enriching region which requires a high number of stages in both cases.

Benzene(1) + hexane(2): values obtained in the simulation of the distillation operation of this binary dissolution are in **Table 6**, while composition and temperature profiles are plotted in **Figure 13**. For the first three *results* (1, 2, and 3), the presence of an azeotrope limits the distillate composition. Thus, *result 1* produces an effluent with a benzene composition of 16.7% (v/v), while for *results 2* and 3, the compositions are, respectively, 37.2 and 30.9%. The simulation carried out with the parametrization of *result 4* produces a purer distillate of 15.6%, due to the absence of the azeotrope. However, the folding effect observed between the equilibrium curves in experimental data as well as the diagram estimated by *result 4* complicates the separation beyond this point. This justifies that the composition profiles are similar to results 1 and 4 (see **Figure 13**).

The residual streams obtained by *results 1* and 4 contain benzene with a purity higher than 99.9%, while the other two *results* do not produce the separation of the

Stage	Result 1 (M2)			Result 2 (M1)			Result 3 (M1)			Result 4 (M1)		
	x_1	y_1	T/K									
1	0.167	0.161	341.3	0.372	0.372	337.3	0.310	0.309	340.1	0.167	0.156	341.7
5	0.201	0.189	341.3	0.372	0.372	337.3	0.312	0.311	340.1	0.220	0.202	341.9
10	0.280	0.250	341.6	0.372	0.372	337.3	0.319	0.316	340.1	0.310	0.278	342.2
15	0.505	0.414	343.1	0.374	0.373	337.3	0.337	0.330	340.1	0.473	0.407	343.2
20	0.842	0.740	348.5	0.405	0.388	337.4	0.392	0.369	340.2	0.772	0.663	346.8
25	0.991	0.982	352.6	0.409	0.390	337.4	0.422	0.389	340.3	0.988	0.975	352.4
30	1.000	0.999	352.8	0.692	0.510	338.8	0.785	0.631	344.0	1.000	0.999	352.8
Q_c /kJ h ⁻¹	1.829E5			1.988E5			1.686E5			1.804E5		
Q_r /kJ h ⁻¹	1.886E5			2.050E5			1.802E5			1.898E5		

Table 6. Quantities obtained in the simulation of a distillation process for the binary benzene(1) + hexane(2), using different values from the efficient front shown in **Figure 9**.

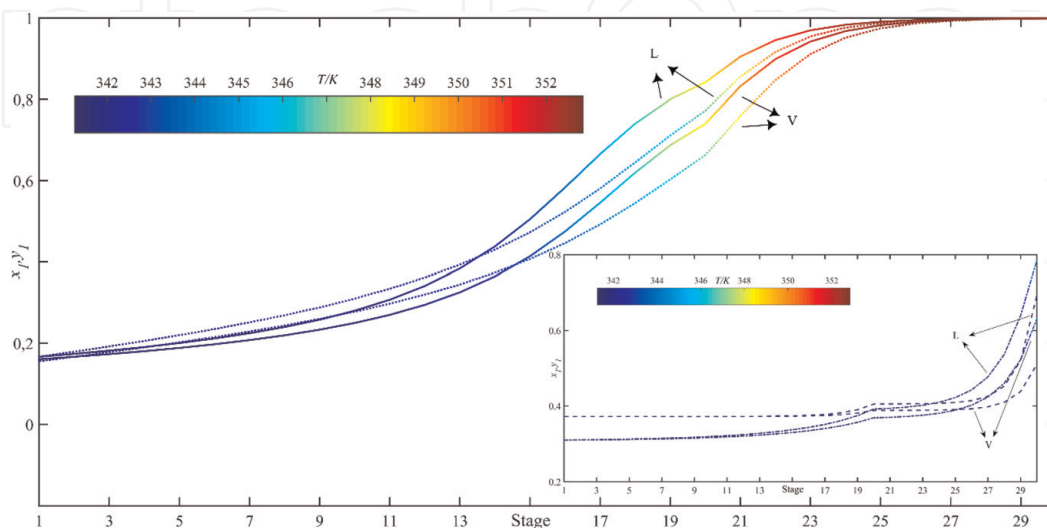


Figure 13. Plot of composition and temperature profiles obtained in the simulation of a separation operation for the binary benzene(1) + hexane(2), using the different parametrizations proposed: (—) 1 (M2); (---) 2 (M1); (.....) 4 (M1). L, liquid stream profile; V, vapor stream profile.

binary dissolution with high purities (no more than 79%), due to the presence of the azeotrope at intermediate composition. The differences noted in compositions in the head and bottom of the column cause that the corresponding temperatures are also different. Between *results* 1 and 4, there is a difference in temperature of almost 0.5 K, while *results* 2 and 3 estimate lower temperatures by more than 1 K with respect to the others. In this case, the modeling errors in another of properties, such as excess enthalpies, as well as the differences in the output composition, also affects to produce noteworthy differences in the energetic consumptions of both condenser and boiler. In this sense, similar results are obtained for *results* 1 and 4, although, a priori, it is not possible to indicate which of these is closer to the true behavior of the column.

5. Conclusions

The aim of this work is to present the practice carried out on a set of operations constituting a procedure involving the following sequences: experimentation \leftrightarrow verification \leftrightarrow modeling \leftrightarrow simulation. A description of the last three operations is proposed since the necessary experimental information (iso- p and iso- T VLE data and h^E) was extracted from the available publications. The proposed methodology is applied to two significant binary systems in the dissolution thermodynamic field, such as acetone-ethanol and benzene-hexane. The data checking is carried out with different classical methods, which is recommended in the recent literature [6]. In addition, a rigorous method recently designed by the authors [7] was also used in order to guarantee the quality of the experimental data used. This method has the advantage of offering some information about the origin of deficiencies in the experimental data.

A polynomial expression was used in the *modeling* step (see Eqs. (1) and (3)), used in the correlation of thermodynamic properties, from which four sub-models (M1–M4) are established in Section 2.1, depending on the availability of data for each system to avoid overfitting. Modeling in all cases was performed on the Gibbs dimensionless function, g^E/RT (VLE), and on h^E data, two-objective optimization approach addressed as a sequence of mono-objective subproblems according to the ϵ -constraint algorithm. A set of models are selected from the attained *efficient fronts* to provide a rationale on the trade-off decision task that is supposed to yield the final model for later uses, such as design/simulation. For the two studied cases, these *fronts* reveal a quasi-linear trend (with a negative slope) when the number of parameters used in the model is small. *Efficient fronts*' slope decreases as the number of parameters increases, until the error of VLE delinks to that of the h^E for highly flexible models.

The rectification of the selected systems was simulated using the *RadFrac* block of AspenPlus[®] with the selected thermodynamic parametrizations. For the binary acetone + ethanol, some models showed an immiscible region, not reflected by the experimental information, giving rise to incoherent simulations. Two models gave rise to inexistent azeotropes in the benzene + hexane dissolution, with incorrect results in the simulation. On the other hand, errors in the excess enthalpy estimates did not influence on the procedure simulation, but it should be noted that it has an important role in the modeling of binary systems. In summary, the influence of a certain set of parameters on the simulation varies depending on each particular system. Besides, it is observed that, as the number of parameters grows in a model, the optimization problem mutes toward a mono-objective one since the considered criteria are invariant in one another. In these cases, taking the set of parameters that present the lowest error on h^E is the best option. However, increasing the number of parameters might lead to overfitting if not enough attention is paid to the model extrapolation capabilities.

Acknowledgements

This work was supported by the Ministerio de Economía y Competitividad (MINECO) of the Spanish Government, Grant CTQ2015-68428-P. One of us (AS) is also grateful to the ACIISI (from Canaries Government, No. 2015010110) for the support received. This work is a result of the Project “AIProcMat@N2020—Advanced Industrial Processes and Materials for a Sustainable Northern Region of Portugal 2020,” with the reference NORTE-01-0145-FEDER-000006, supported by Norte Portugal Regional Operational Programme (NORTE 2020), under the Portugal 2020 Partnership Agreement, through the European Regional Development Fund (ERDF); Associate Laboratory LSRE-LCM—UID/EQU/50020/2019—funded by national funds through FCT/MCTES (PIDDAC).

A. Vapor pressure modeling

Vapor pressures of pure compounds are calculated using Antoine equation:

$$\log p_i^{\circ}/kPa = A - B/[T/K - C] \quad (10)$$

Parameters A , B , and C , from literature [60–62], are shown in **Table A1**.

	A	B	C	Ref.
Acetone	6.42448	1312.25	32.45	[60]
Ethanol	7.24677	1598.67	46.42	[61]
Benzene	6.03053	1211.03	52.36	[62]
Hexane	5.87891	1089.49	60.55	[62]

Table A1.
Parameters of Antoine equation for pure compounds in this work.

Author details

Adriel Sosa¹, Luís Fernández¹, Elena Gómez², Eugénia A. Macedo² and Juan Ortega^{2*}

¹ Grupo de Ingeniería Térmica e Instrumentación (IDeTIC), Parque Científico-Tecnológico, Universidad de Las Palmas de Gran Canaria, Canary Islands, Spain

² Associate Laboratory of Separation and Reaction Engineering and Laboratory of Catalysis and Materials (LSRE-LCM), Department of Chemical Engineering, Faculty of Engineering, University of Porto, Porto, Portugal

*Address all correspondence to: juan.ortega@ulpgc.es

IntechOpen

© 2019 The Author(s). Licensee IntechOpen. This chapter is distributed under the terms of the Creative Commons Attribution License (<http://creativecommons.org/licenses/by/3.0/>), which permits unrestricted use, distribution, and reproduction in any medium, provided the original work is properly cited. 

References

- [1] Luyben WL. Process Modeling, Simulation and Control for Chemical Engineers. 2nd ed. New York: McGraw-Hill; 1989
- [2] Turton R, Baille RC, Whiting WB, Shaelwitz JA. Analysis, Synthesis, and Design of Chemical Processes. 3th ed. Boston: Prentice Hall; 1998
- [3] Coello C, Lamont G, Van Veldhuisen D. Evolutionary Algorithms for Solving Multi-objective Problems. 2nd ed. Berlin: Springer; 2007
- [4] Nocedal J, Wright SJ. Numerical Optimization. 2nd ed. Berlin: Springer; 2006
- [5] Deb K. Multi-Objective Optimization Using Evolutionary Algorithms. New Jersey: Wiley; 2001
- [6] Wisniak J, Ortega J, Fernández L. A fresh look at the thermodynamic consistency of vapor-liquid equilibria data. The Journal of Chemical Thermodynamics. 2016;105:355-365
- [7] Fernández L, Ortega J, Wisniak J. A rigorous method to evaluate the consistency of experimental data in phase equilibria. Application to VLE and VLLE. AIChE Journal. 2017;63:5125-5148
- [8] Ortega J, Espiau F, Wisniak J. New parametric model to correlate the excess Gibbs function and thermodynamic properties of multicomponent systems. Application to binary systems. Industrial and Engineering Chemistry Research. 2010;49:406-421
- [9] Lagarias JC, Reeds JA, Wright MH, Wright PE. Convergence properties of the Nelder-Mead simplex method in low dimensions. SIAM Journal on Optimization. 1998;9:112-147
- [10] Chu JC, Getty RJ, Brennecke JF, Paul R. Distillation Equilibrium Data. New York: Reinhold; 1950
- [11] Hellwig LR, Van Winkle M. Vapour-liquid equilibria for ethyl alcohol binary systems. Industrial and Engineering Chemistry. 1953;45:624-629
- [12] Amer HH, Paxton RR, Van Winkle M. Methanol-ethanol-acetone vapor-liquid equilibria. Industrial and Engineering Chemistry. 1956;48:142-146
- [13] Morachevskii AG, Leontév NP. Liquid vapor equilibrium in the ternary system acetone chloroform ethyl alcohol. Zhurnal Fizicheskoi Khimii. 1960;34:2347-2349
- [14] Vinichenko IG, Susarev MP. Study and calculation of the liquid-vapor equilibrium in the acetone-ethanol-hexane system. Zhurnal Prikladnoi Khimii. 1966;39:1583-1587
- [15] Ku H-C, Tu C-H. Isobaric vapor liquid equilibria for mixtures of acetone, ethanol, and 2,2,4-trimethylpentane at 101.3 kPa. Fluid Phase Equilibria. 2005; 231:99-108
- [16] Chen S, Bao Z, Lu Z, Yang Y, Xu W, Chen Z, et al. Vapor liquid equilibrium for the 1,1,1-trifluoroethane + sulfur dioxide system at 101.3 kPa. Journal of Chemical & Engineering Data. 2014;59:16-21
- [17] Kato M. Analysis of the excess Gibbs energies of binary mixtures using non-randomness factors determined from excess volume data. Bulletin of the Chemical Society of Japan. 1982;55:23-27
- [18] Campbell SW, Wilsak RA, Thodos G. Vapor-liquid equilibrium measurements for the ethanol-acetone

system at 327.7, 397.7, and 422.6 K. *Journal of Chemical & Engineering Data*. 1987;**32**:357-362

[19] Lee MJ, Hu C-H. Isothermal vapor-liquid equilibria for mixtures of ethanol, acetone, and diisopropyl ether. *Fluid Phase Equilibria*. 1995;**109**:83-98

[20] Paz-Andrade MI, Jimenez E, Lopez-Garcia D. Excess enthalpies for the systems acetone + ethanol, acetone + 1-pentanol and acetone + 1-hexanol at 25 c. *Anales de Quimica*. 1973;**69**:289-294

[21] Coomber BA, Wormald CJ. A stirred flow calorimeter: The excess enthalpies of acetone+water and of acetone+some normal alcohols. *The Journal of Chemical Thermodynamics*. 1976;**8**: 793-799

[22] Nicolaidis GL, Eckert CA. Experimental heats of mixing of some miscible and partially miscible nonelectrolyte systems. *Journal of Chemical & Engineering Data*. 1978;**23**: 152-156

[23] Lietzmann A, Loewen B, Schulz S. Excess molar enthalpies of propanone + heptane, propanone + ethanol, ethanol + heptane, and 2-propanol + water at 283.15, 298.15, 323.15, 343.15, and 363.15 K. *Journal of Chemical & Engineering Data*. 1994;**39**:785-788

[24] Nagata I, Ksiazczak A. Excess enthalpies for (ethanol + propanone) and (ethanol + propanone + benzene) at the temperature 298.15 K. *The Journal of Chemical Thermodynamics*. 1994;**26**: 165-169

[25] Lien P-J, Lin HM, Lee MJ. Excess molar enthalpies for binary mixtures of ethanol + acetone, +octane, +cyclohexane and 1-propanol + acetone, +octane, +heptane at 323.15 K. *Journal of Chemical & Engineering Data*. 2003;**48**: 359-361

[26] Tongberg CO, Johnston F. Vapor-liquid equilibria for n-hexane-benzene mixtures. *Industrial and Engineering Chemistry*. 1933;**25**:733-735

[27] Myers HS. Vapor-liquid equilibrium data for binary mixtures of paraffins and aromatics. *Industrial and Engineering Chemistry*. 1955;**47**: 2215-2219

[28] Kumarkrishna Rao VN, Swami DR, Narasinga Rao N. Vapor-liquid equilibria of benzene-hexane and benzene-cyclohexane systems. *AIChE Journal*. 1957;**3**:191-197

[29] Gothard F, Minea I. *Revista De Chimie*. 1960;**11**:642

[30] Gothard F, Minea I, Grigoras C. *Revista De Chimie*. 1960;**11**:705

[31] Brzostowski W. Vapor-liquid equilibria in the benzene + hexane system containing carbon 14-labelled benzene. *Bull. Acad. Pol. Sci.-Chim*. 1961;**9**:471-475

[32] Gothard F, Minea I. Rectification of n-hexane + benzene mixtures and the liquid-vapor equilibrium of these mixtures. *Revista De Chimie*. 1961;**12**: 489-493

[33] Gothard F, Minea I. Vapor-liquid equilibrium of hexane+benzene mixtures at low pressures. *Revista De Chimie*. 1963;**14**:520-525

[34] Butler PA, Ridgway K. Ternary vapour-liquid equilibrium: The use of a multi-stage still. *Journal of Applied Chemistry*. 1967;**17**:191-197

[35] Hanson DO, Van Winkle M. Alteration of the relative volatility of n-hexane-1-hexene by oxygenated and chlorinated solvents. *Journal of Chemical & Engineering Data*. 1967;**12**: 319

- [36] Ridgway K, Butler PA. Some physical properties of the ternary system benzene-cyclohexane-n-hexane. *Journal of Chemical & Engineering Data*. 1967;12:509-515
- [37] Michishita T, Arai Y, Saito S. Vapor-liquid equilibria of hydrocarbons at atmospheric pressure. *Kagaku Kogaku*. 1971;35:111-116
- [38] Barhala A, Gothard FA, Marchidan DI. Liquid-vapor equilibria in binary mixtures of 2-chlorotoluene + 4-chlorotoluene and toluene + 2-chlorotoluene. *Revue Roumaine de Chimie*. 1992;37:27-40
- [39] Susarev MP, Chen S-T. Calculation of liquid-vapor equilibrium for ternary systems from data on binary systems—the system benzene-n-hexane-cyclohexane. *Zhurnal Fizicheskoi Khimii*. 1963;37:1739-1744
- [40] Beyer W, Schubert H, Leibnitz E. *Journal für Praktische Chemie*. 1965;27:276
- [41] Li IPC, Wong YW, Chang S-D, Lu BC-Y. Vapor-liquid equilibria in systems n-hexane-benzene and n-pentane-toluene. *Journal of Chemical & Engineering Data*. 1972;17:492-498
- [42] Saez C, Compostizo A, Rubio RG, Crespo-Colin A, Diaz Pena M. p , T , x , y , data of benzene + n-hexane and cyclohexane + n-heptane systems. *Fluid Phase Equilibria*. 1985;24:241-258
- [43] Baud E. Thermodynamic analysis of binary mixtures. *Bulletin de la Société Chimique de France*. 1915;17:329-345
- [44] Kireev VA. Heats of mixing of liquids. 3. Integral and partial heats of mixing of normal liquids. *Acta Physicochimica URSS*. 1937;7:363-373
- [45] Kuhn W, Massini P. Heat of mixing and azeotrope formation in non-polar liquids. *Helvetica Chimica Acta*. 1950;33:737-765
- [46] Mathieson AR, Thynne JC. Thermodynamics of hydrocarbon mixtures. II. The heats of mixing of the binary mixtures formed by benzene, cyclohexane, heptane, toluene, and hexane. *Journal of the Chemical Society*. 1956:3708-3713
- [47] Schnaible HW, Van Ness HC, Smith JM. Heats of mixing of liquids. *AIChE Journal*. 1957;3:147-152
- [48] Jones HKD, Lu BC-Y. Heats of mixing of liquids for the system ethanol-benzene-n-hexane. *Journal of Chemical & Engineering Data*. 1966;11:488-492
- [49] Paz Andrade MI, Regueiro M, Baluja MC, Jimenez Cuesta E, Hernandez C. Heats of mixing at mean temperatures hexane+benzene system. *Acta Científica Compostelana*. 1970;7:147-154
- [50] Paz Andrade MI. *International DATA Series, Selected Data on Mixtures, Series A*. 1973;2:97-104
- [51] Diaz Pena M, Menduina C. Excess enthalpies at 323.15 K of binary mixtures of benzene with n-alkanes. *The Journal of Chemical Thermodynamics*. 1974;6:1097-1102
- [52] Romani L, Paz Andrade MI. Thermodynamic excess functions at 25 C. III. benzene+hexane isomers. *Anales de Química*. 1974;70:422-425
- [53] Christensen C, Gmehling J, Rasmussen P, Weidlich U. Heats of mixture data collection. In: *DECHEMA Chemistry Data Series. Vol. III*. Frankfurt/Main; 1984
- [54] Bao J, Xie Y, Zhang K, Hu Y. A study on the excess enthalpies for the ternary system benzene-cyclohexane-n-hexane. *Huadong Huagong Xueyuan Xuebao*. 1985;11:467-478
- [55] Hwang C-A, Elkabule AS, Whitman DL, Miller RC. Excess molar enthalpies of (benzene + cyclohexane + n-hexane).

The Journal of Chemical
Thermodynamics. 1987;**19**:1031-1036

[56] Casado H, Segade L, Franjo C,
Jimenez E, Paz Andrade MI. Excess
molar enthalpies of propyl propanoate +
hexane + benzene at 298.15 and 308.15
K. Journal of Chemical & Engineering
Data. 2000;**45**:445-449

[57] Mato MM, Balseiro J, Jimenez E,
Legido JL, Galinanes AV, Paz-Andrade
MI. Excess molar enthalpies and excess
molar volumes of the ternary system
1,2-dichlorobenzene+benzene+hexane
at 298.15 K. Journal of Chemical &
Engineering Data. 2002;**47**:1436-1441

[58] Yi CK, Park Y, You S-S.
Measurement of excess enthalpies using
a high-pressure flow microcalorimeter
and determination of binary interaction
parameters for thermodynamic models.
Korean Journal of Chemical
Engineering. 2009;**26**:220-224

[59] Aspen Technologies Inc. Aspen
Physical Properties System. UK:
Cambridge; 2004

[60] Ambrose D, Sprake CHS, Townsend
R. Thermodynamic properties of
organic oxygen compounds XXXIII. The
vapour pressure of acetone. The Journal
of Chemical Thermodynamics. 1974;**6**:
693-700

[61] Ambrose D, Sprake CHS.
Thermodynamic properties of organic
oxygen compounds XXV. Vapour
pressures and normal boiling
temperatures of aliphatic alcohols. The
Journal of Chemical Thermodynamics.
1970;**2**:631-645

[62] Riddick JA, Bunger WB, Sakano TK.
Organic solvents: Physical properties
and methods of purification. In:
Techniques of Chemistry. 4th ed. Vol. II.
New York: Wiley-Interscience; 1986